Degradation Behavior of 850 nm AlGaAs/GaAs Oxide VCSELs Suffered from Electrostatic Discharge

Taeyong Kim, Taeki Kim, Sangin Kim, and Sang-Bae Kim

The effect of forward and reverse electrostatic discharge (ESD) on the electro-optical characteristics of oxide vertical-cavity surface-emitting lasers is investigated using a human body model for the purpose of understanding degradation behavior. Forward ESD-induced degradation is complicated, showing three degradation phases depending on ESD voltage, while reverse ESD-induced degradation is relatively simple, exhibiting two phases of degradation divided by a sudden distinctive change in electro-optical characteristics. We demonstrate that the increase in the threshold current is mainly due to the increase in leakage current, nonradiative recombination current, and optical loss. The decrease in the slope efficiency is mainly due to the increase in optical loss.

Keywords: Vertical-cavity surface-emitting laser, semiconductor laser, electrostatic discharge, semiconductor device reliability.

I. Introduction

Vertical-cavity surface-emitting lasers (VCSELs) have been consolidating their position as a major active device in local area networks due to their low cost and high performance. A variety of applications related to short distance links are increasingly open to VCSELs, such as polymer waveguides [1], free-space optics [2], [3], and sensors [4], while gigabit Ethernet and fiber channel applications are leading the current market of VCSELs. VCSELs have many unique features making all of these possible, namely, low-cost mass production, small-scale integration including VCSEL arrays, high reliability, and low power consumption.

However, reliability problems associated with electrostatic discharge (ESD) still remain the most critical issue to be solved for further deployment of VCSELs in various applications. Since the active area of VCSELs is much smaller than that of edge-emitting lasers, the sensitivity to ESD is much higher [5]-[8]. In particular, this problem is more serious in oxide VCSELs than in implanted VCSELs due to the smaller active area of oxide VCSELs and the defects and stress originating from the oxide layer. The ESD-induced damage threshold of commercially available oxide VCSELs is up to around 300 V [9], [10]. A series of ESD tests on oxide VCSELs using a human body model [11], a machine model, and a charged device model were performed in order to grasp a material-level understanding of ESD-induced behavior. The VCSELs subjected to ESD were analyzed using focused ion beam microscopy together with transmission electron microscopy [12]-[14]. It was reported that the ESD events generated dislocation tangles with different shapes and locations, and most of the ESD-induced degradation originated from the oxide layer.

Manuscript received Mar. 6, 2008; revised Aug. 28, 2008; accepted Oct. 9, 2008.
This work was supported in part by the BK21 program of the Korea Ministry of Education.
Taeyong Kim (phone: +82 31 219 2484, email:otherwisekay@gmail.com), Taeki Kim (email: tkkim1127@gmail.com), Sangin Kim (email: sangin@ajou.ac.kr), and Sang-Bae Kim (email: sbkim@ajou.ac.kr) are with the Division of Electrical and Computer Engineering, Ajou University, Suwon, Rep. of Korea.

Reverse current voltage (I-V) characteristics are now widely used to check VCSELs for ESD-induced defects and failures since the reverse leakage current is one of the characteristics most sensitive to ESD exposure [10]. In addition to I-V measurement, more precise and comprehensive understanding of ESD-induced degradation was achieved by employing electroluminescence (EL) microscopy and emission microscopy [13].

On the other hand, estimating the ESD threshold and screening out ESD-damaged devices by using non-destructive methods are more important to both users and manufacturers. The effect of forward and reverse ESD on proton implanted VCSELs was investigated using light output power-current-voltage (L-I-V) measurement, as well as optical spectrum and optical emission transient measurements [15]. It was found that the degradation of the optical properties preceded the electrical properties during the forward ESD test, and the reverse ESD-induced degradation started at a lower ESD voltage. Reverse ESD stress results in a sudden increase in the reverse current compared to the forward bias stress. Several studies have been published on the ESD sensitivity of oxide VCSELs [9], [10], [13], [14]. Nevertheless, no clear analysis has been carried out to understand the cause of ESD-induced deterioration and the development of VCSEL characteristics with increases in ESD voltage.

The purpose of this paper is to clarify the development of the electrical and optical characteristics with increases in the forward and reverse ESD voltage. For this purpose we analyze the electrical and optical characteristics of oxide VCSELs by applying sequentially increasing ESD voltage.

A brief description of the tested devices and the ESD test setup is given in section II. Then, the changes in electro-optical characteristics induced by both forward and reverse ESD are presented with the emphasis on the degradation phase in section III, followed by conclusions in section IV. This study demonstrates that forward ESD-induced degradation goes through three distinctive phases as the ESD voltage increases, while reverse ESD-induced degradation shows sudden abrupt changes in the electro-optical characteristics. The results make it possible to distinguish between damaged and undamaged VCSELs.

II. Test Setup and Procedure

The oxide VCSELs used in this study consist of P-type distributed Bragg reflector (DBR) mirror layers, N-type DBR mirror layers, and 1–λ cavity sandwiched by the two DBR mirror layers. Each device was mounted on a TO header without a cap in order to observe the surface of the device and the EL pattern easily. All the tests and device characterization were performed at room temperature without any stabilization process such as burn-in. The oxide aperture diameter of the tested devices ranges from 9.8 μm to 10.2 μm, with an average of 10 μm. The average threshold current and slope efficiency of the devices are 1 mA and 0.55 W/A, respectively. The average lasing wavelength at room temperature is 845 nm, and it has a temperature coefficient of 0.06 nm/ºC. The devices are commercially available from CTS Inc.

A NOISEKEN ESS-606 simulator was used to generate ESD pulses, and the simulator conforms to the MIL-STD-883D human body model and machine model. To observe the development of electrical and optical characteristics resulting from ESD-induced degradation, an ESD pulse accumulation test was performed with sequentially increasing ESD voltage by a constant voltage step. At each voltage step, three consecutive ESD pulses with a one-second delay between each pulse were applied in the forward or reverse direction. The voltage step sizes were 200 V and 50 V for forward and reverse directions, respectively. All the devices used in ESD tests were characterized by L-I-V measurement and EL microscopy before and after each application of ESD pulses. Optical spectra were measured at various current levels to observe changes in the VCSEL mode behavior. The light output from each TO-mounted device was directly coupled to the optical spectrum analyzer via multi-mode fiber. The optical emission spectra were measured at room temperature with a wavelength resolution of 0.05 nm.

III. Results and Discussion

1. Changes in the Electro-Optical Characteristics Caused by Forward ESD

Figure 1(a) shows the development of the L-I-V characteristics of device A during the forward ESD pulse accumulation test. The slope efficiency of device A did not change upon the application of 800 V pulses and it started to decrease after the application of 1,000 V pulses, showing a 15% decrease. After the application of 1,000 V pulses, that is, after the first decrease of optical output power was observed, the optical output power continuously and slowly decreased with increasing ESD pulse amplitude. However, the optical output power decreased drastically after the application of 5,800 V pulses. The operating voltage at a given forward current decreased with ESD voltages below the threshold current, while it increased above the threshold current with increasing ESD pulse amplitude. This means that ESD-induced degradation results in increased leakage current and series resistance. Figure 1(b) shows the measured I-V curves from the forward ESD pulse accumulation test. Up to the ESD voltage of 800 V, we could not observe any change in the I-V

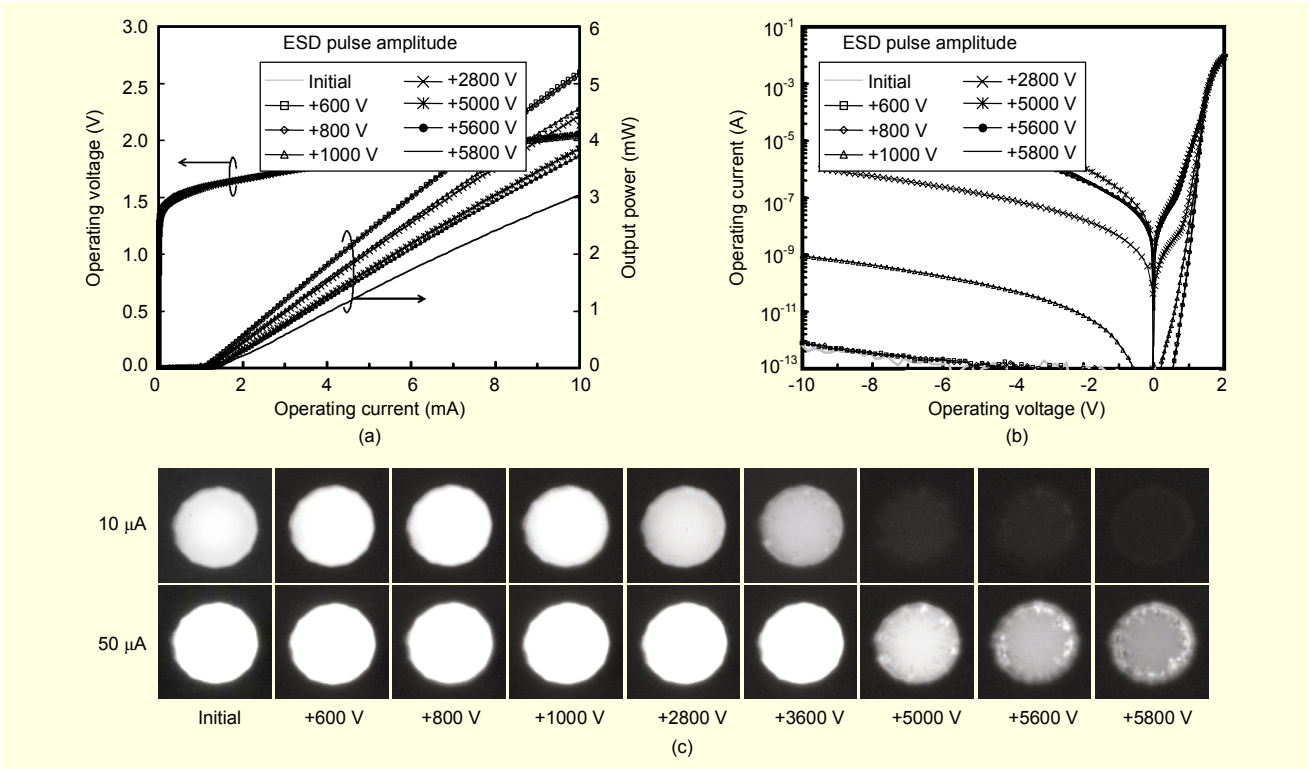

Fig. 1. Development of the forward ESD-induced degradation of device A: (a) L-I-V curves, (b) I-V curves, and (c) EL images at the operating current of 10 μA (upper row) and 50 μA (lower row).

characteristics; however, above 1,000 V, we observed a dramatic increase in the reverse current and the forward current for operating voltages below 1 V. As seen in Fig. 1(b), the reverse current gradually increased as the ESD voltage increased further. The reverse current at the operating voltage of –2 V just after the application of 800 V ESD pulses is about 0.8 pA, and it reaches 7.22 pA and 1 μA after the application of 1,000 V and 5,000 V ESD pulses, respectively. The forward and reverse currents show symmetry with respect to the 0 V axis for operating voltages from –0.5 V to 0.5 V. This means that the resistive leakage current component is dominant in the total current at low operating voltages. Figure 1(c) shows EL images at the operating current of 10 μA and 50 μA. After the application of 1,000 V ESD pulses, where degradation started to occur, the edges of the active area started to darken. Overall darkening was observed after the application of 2,800 V ESD pulses, and clear dark spots appeared when the ESD voltage was 5,000 V. Above 5,000 V, dark spots and bright white speckles appeared along the edge. After ESD voltage reached 5,000 V, little light could be observed at the operating current of 10 μA. This means that the ESD-induced degradation at this voltage seriously damages the whole active area including the edge region. The degradation of the whole active area is revealed by the increased nonradiative current and decreased radiative current components, which will be discussed in III.3.

Figure 2(a) shows the slope efficiency (*dL/dI*) measured during the forward ESD pulse accumulation test. When the ESD voltage was less than 800 V, we could only observe a small amount of fluctuation in *dL/dI*. Then, *dL/dI* started to decrease after the application of 1,000 V ESD pulses and continuously decreased with further increase in the ESD voltage. In particular, *dL/dI* around the threshold unevenly varied during the forward ESD accumulation test. This is due to the mode-dependent increase in absorption and subsequent changes the mode behavior resulting from damage in the active area and adjacent areas. It is well known that changes in the spatial mode behavior of semiconductor lasers have influence on *dL/dI*-I characteristics. To explain the change in *dL/dI*, we measured the optical emission spectra of device A at several operating current levels in the initial state and after the application of 5,800 V pulses. Figure 2(b) shows the optical emission spectra at the operating current of 1.8 mA for the initial state and after the application of 5,800 V pulses. The optical emission spectrum of the initial state showed six peaks, whereas the spectrum after the ESD pulse application showed only a single peak. We also observed that the peak wavelength of the same mode after the application of 5,800 V pulses was shorter than that of the initial state. Both of the optical spectra at operating currents of 2.0 mA and 2.4 mA exhibited six peaks before the application of ESD pulses, and two peaks after the

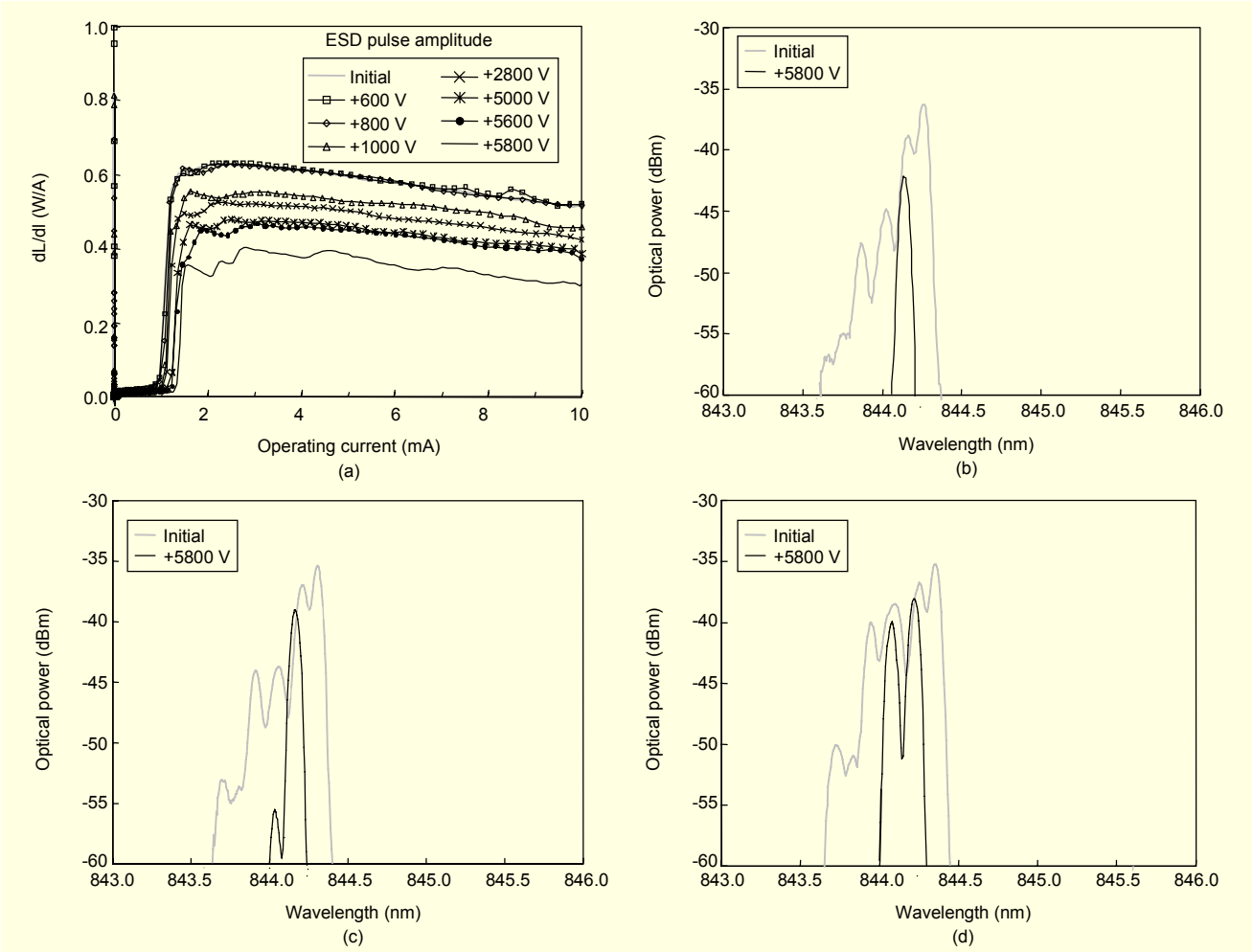

Fig. 2. (a) Development of the slope efficiency (*dL*/*dI*) of device A during forward ESD pulse accumulation test. Measured optical spectra before and after ESD test: at the operating current of (b) 1.8 mA, (c) 2.0 mA, and (d) 2.4 mA, respectively.

Table 1. Peak wavelength (nm) before and after the ESD-induced degradation at each operating current (mA).

Forward ESD			Reverse ESD		
Current	Before	After	Current	Before	After
1.8	844.17	844.15	2.0	845.99	845.89
2.0	844.22	844.17	3.0	846.16	846.10
2.4	844.26	844.23	3.4	846.36	846.32

application of the ESD pulses. This means that ESD-induced degradation occurs mainly along the edge of the active area adjacent to the oxidized region, resulting in a reduction of the effective active area. Therefore, the reduced effective active area leads to a decrease in the effective refractive index, resulting in a blue shift in the lasing spectrum. The peak wavelengths at given operating currents before and after ESD-induced degradation are listed in Table 1. For the same reason, the number of lasing modes also decreases. It should be noted that kinks in *dL*/*dI* curves are associated with the lasing of higher order spatial modes.

2. Changes in the Electro-Optical Characteristics Caused by Reverse ESD

Figure 3(a) shows the development of the L-I-V characteristics of device B during the reverse ESD pulse accumulation test. We could see no change in the L-I-V characteristics up to the ESD voltage of –200 V. After the application of –250 V pulses, the optical output power started to decrease, and the slope efficiency decreased by 24%. After the application –400 V ESD pulses, the slope efficiency decreased to 50% of the initial value. The threshold current showed less change than the observed threshold current change during the forward ESD pulse accumulation test. Up to an ESD voltage of –200 V, we could see no change in the threshold current. However, after the

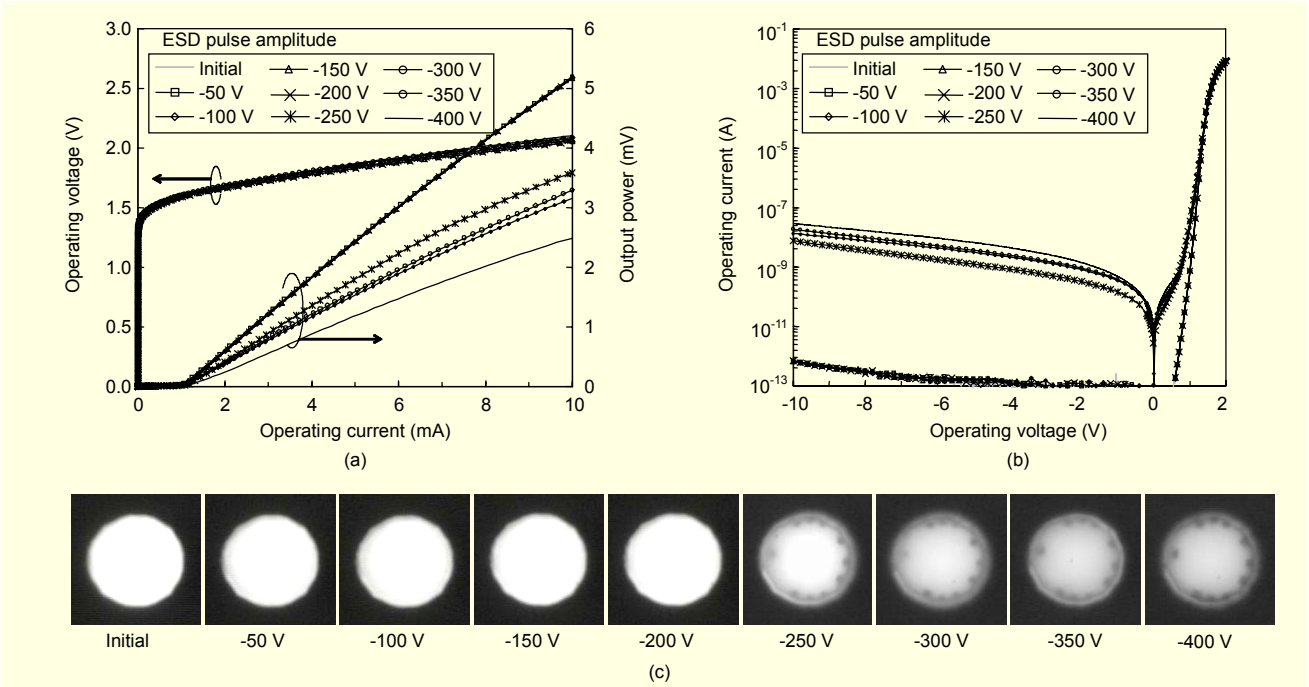

Fig. 3. Development of the reverse ESD-induced degradation of device B: (a) L-I-V characteristics, (b) I-V characteristics, and (c) EL images at the operating current of 10 μA.

application of –250 V pulses, the threshold current increased from 1.077 mA to 1.119 mA. With further increase in the reverse ESD voltage, the threshold current did not show any drastic change. This can be explained by the mutually compensating effect of the increased optical absorption and the decreased effective active area.

The development of the I-V characteristics during the reverse ESD pulse accumulation test is shown in Fig. 3(b). The reverse current at the operating voltage of –2 V stayed below 1 pA up to the ESD voltage of –200 V; however, it increased drastically up to 1 nA after the application of –250 V pulses. For higher reverse ESD voltage after the application of –250 V pulses, the reverse leakage current increased slowly. It is interesting that the reverse current during the forward ESD pulse accumulation test continued to increase, whereas it tended to saturate during the reverse ESD pulse accumulation test. Figure 3(c) shows EL images of device B during the reverse ESD pulse accumulation test. The emission light intensity of device B shown in Fig. 3(c) started to decrease and the dark spots along the edge of the active region appeared suddenly after the application of –250 V pulses. With further applications of increased ESD pulses after the first observable ESD-induced degradation, the dark spots gradually darkened; however, the EL intensity from the central area did not change. Also, no new dark spots were generated. It can be concluded that the initially generated leakage path associated with the dark spots bypassed the reverse current due to the reverse ESD voltage, which provided sufficient parallel current paths. In consequence, the number and location of the dark spots remain unchanged in spite of subsequent higher voltage ESD pulses.

Figure 4(a) shows the *dL/dI*-I characteristics during the reverse ESD pulse accumulation test. We could see no change in *dL/dI*-I characteristics up to the ESD voltage of –200 V. After the application of –250 V ESD pulses, *dL/dI* dramatically decreased by 24%, and kinks at 1.71 mA and 2.14 mA could be clearly distinguished. As the ESD voltage increased further, the average slope efficiency continued to decrease, and the position of the kinks in the *dL/dI*-I curve shifted to higher currents. To investigate the spatial mode behavior before and after the application of reverse ESD pulses, we measured the optical spectrum of device B in the same manner as in the forward ESD pulse accumulation test. The optical spectra before and after the application of –400 V pulses were measured at several operating current levels. As seen in Fig. 4(b), the optical spectrum of the initial state shows multi-mode behavior with three peaks, while the ESD-damaged spectrum shows only a single peak.

Similar to the results observed in Fig. 2(b), and as can be seen in Fig. 3(c), the application of reverse ESD pulses seriously damages the edge of the active region along the oxide edge, resulting in a reduction of the effective active area. In summary, ESD-induced damage leads to increased series resistance and leakage current, a wider single-mode operation range, and a blue shift in the laser spectra.

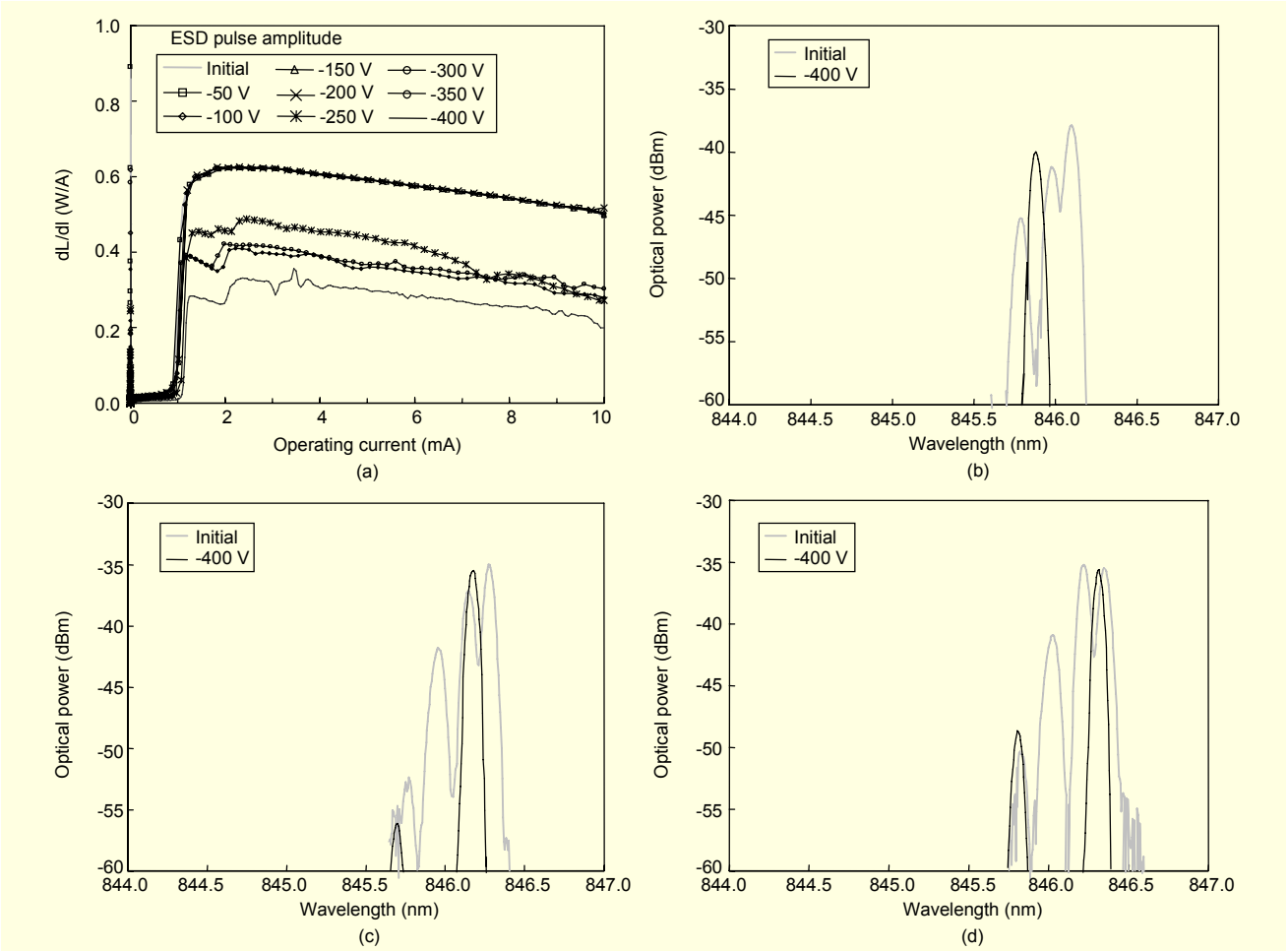

Fig. 4. (a) Development of the slope efficiency (*dL/dI*) of device B during reverse ESD pulse accumulation test. Measured optical spectra before and after ESD test: at the operating current of (b) 2.0 mA, (c) 3.0 mA, and (d) 3.4 mA, respectively.

3. Development of Forward ESD-Induced Degradation

Figure 5(a) shows the forward ESD-induced change in the reverse current at the operating voltage of –2 V and the slope efficiency *dL/dI* at the operating current of 3 mA for three different devices. Figure 5(b) shows the development of the normalized threshold current for the three devices. As shown in Fig. 5(a), the reverse current at the operating voltage of –2 V stayed below 1 pA before the ESD test. However, the reverse current of the three devices rapidly increased and the slope efficiency *dL/dI* at the operating current of 3 mA decreased by more than 10% after the application of 1,000 V ESD pulses. As the ESD voltage increased to 1,600 V, the reverse current at the operating voltage of –2 V exponentially increased and reached 0.1 nA at 1,600 V. The reverse current at the operating voltage of –2 V nearly linearly increased with the ESD voltage in the ESD voltage range from 1,600 V to 5800 V and was greater than 100 nA at the ESD voltage of 5,800 V. On the other hand, the development of *dL/dI* at the operating current of 3 mA shows a different behavior than the reverse current. As shown in Fig. 5(a), at the operating current of 3 mA, *dL/dI* of the three devices dropped by approximately 0.05 W/A after the application of 1,000 V ESD pulses and then decreased relatively slowly with increasing forward ESD voltage up to about 5,000 V. At 4,600 V, *dL/dI* at the operating current of 3 mA of one device suddenly decreased while that of the other two devices maintained the same rate of decrease up to 5,200 V and 5,800 V, respectively. In Fig. 5(b) the normalized threshold current shows a slight fluctuation up to the application of 1,000 V ESD pulses. This fluctuation can be attributed to the fact that the devices were not stabilized at all.

In the ESD voltage range from 1,000 V to 5,000 V, the threshold current slowly increased after a small sudden increase at 1,000 V, which is similar to the pace of *dL/dI* change shown in Fig. 5(a). A sudden increase in the threshold current at around 5,000 V occurred simultaneously with the drastic decrease in *dL/dI*, indicating that the underlying reason for the change is the increased optical absorption. The

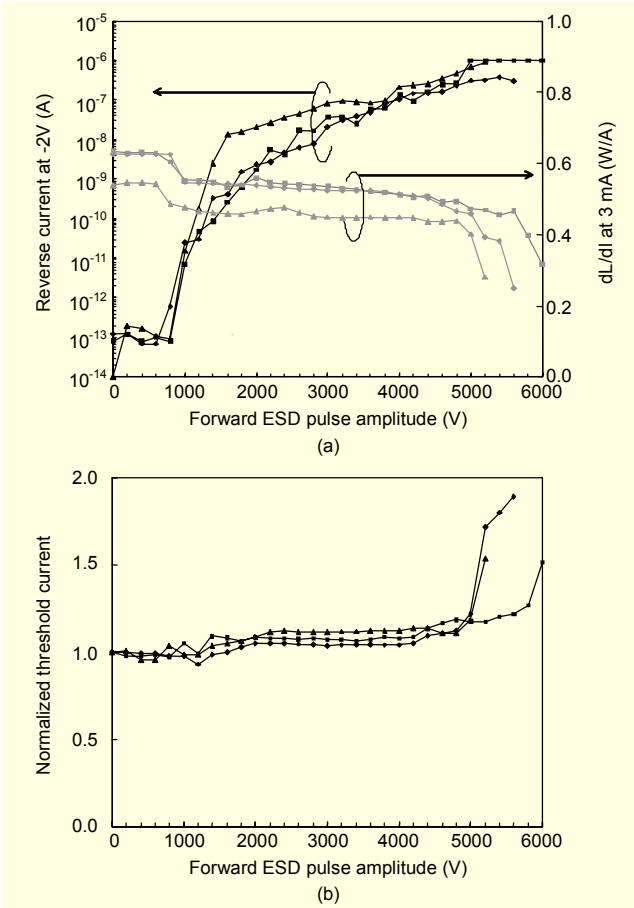

Fig. 5. Development of (a) the reverse current at the operating voltage of –2 V with slope efficiency *dL*/*dI* at 3 mA and (b) the normalized threshold current of three devices during the forward ESD pulse accumulation test. Black lines denote the development of the reverse current. Gray lines denote the development of *dL*/*dI* in (a).

application of ESD pulses of 5,000 V and higher damages the entire active region as well as the edge of the active region as can be seen in the EL images in Fig. 1(c); thus, the degradation at this voltage range causes the decrease in *dL*/*dI* and the increase in the threshold current.

To clarify the mechanism underlying the ESD-induced degradation of oxide VCSELs, we have analyzed the current components of oxide VCSELs using an equivalent circuit model taking into account various current paths. The equivalent circuit model of the oxide VCSEL for this study is shown in Fig. 6. The total current I through the oxide VCSEL consists of the radiative recombination current component I_r, two nonradiative recombination current components I_{nr1} and I_{nr2}, shunted-diode leakage current component I_{lk}, and resistive leakage current component I_{rp}. The radiative current component I_r is separated into parallel paths denoted by D_r and Z_r, where D_r denotes the normal diffusion current, and an ideal Zener diode Z_r represents the junction voltage clamping

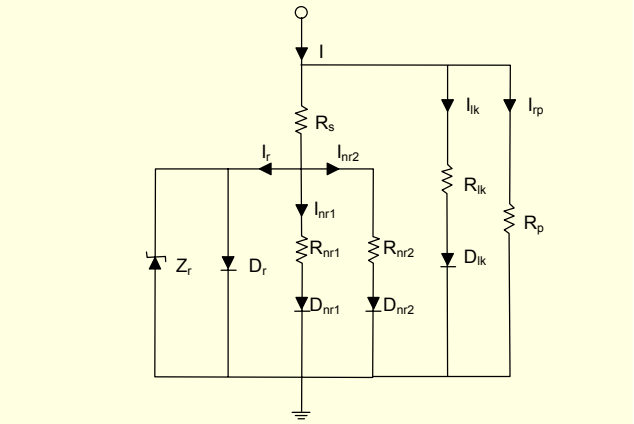

Fig. 6. Equivalent circuit model of the oxide VCSEL.

above the threshold. Two nonradiative recombination current components I_{nr1} and I_{nr2} are modeled using a resistor in series with a diode for each. The resistor R_{nr1} and the diode D_{nr1} are used for I_{nr1}, and the resistor R_{nr2} in series with D_{nr2} is used for the current component I_{nr2}. The series resistance R_s includes the contact, bulk, and interface resistance of P- and N-type DBR mirror layers, and it is modeled using the following expression:

$$R_s = R_c + R_v = R_c + \frac{R_{n0}}{1 + I/I_{n0}}, \quad (1)$$

where R_c is the constant resistance component which is independent of the total current I, and R_v is the current dependent nonlinear resistance component. The nonlinear resistance component R_v is expressed in a fractional form including the nonlinear resistance coefficient R_{n0} and nonlinear current coefficient I_{n0}. To take account of the junction voltage saturation at lasing, we included a parallel Zener diode Z_r with a breakdown voltage of $V_{j,th}$, where $V_{j,th}$ is the lasing threshold voltage across the junction [16], [17].

The analysis results of the forward ESD pulse accumulation test are summarized in Table 2, which lists the model parameters used for the equivalent circuit model. In Table 2, the reverse saturation current I_s of the diode D_r providing the radiative recombination current components I_r shows no change up to the forward ESD voltage of 800 V. It then decreases from 4.0×10^{-25} to 2.1×10^{-25} A and 1.6×10^{-25} A after the application of 1,000 V and 1,200 V ESD pulses, respectively. After exposure to 5,800 V ESD pulses, the reverse saturation current I_s decreases to 3.2×10^{-28} A, which is about 0.1% of the initial value. The ideality factor n is 1.2 in the initial state and gradually decreases with the accumulation of ESD pulses and becomes 1.06 after the application of 5,800 V pulses. The decrease in I_s caused by the forward ESD is attributed mainly to the reduction of the ideality factor n, although the reduction of the effective active area also contributes to the

Table 2. Fitting parameters from the current component analysis using the equivalent circuit model for forward ESD pulse accumulation test, where I_s denotes the reverse saturation current, and n denotes the ideality factor.

Degradation phase		Phase 1	Phase 2				Phase 3
ESD voltage		0 V	+1000 V	+1200 V	+2400 V	+3600 V	+5800 V
D_r	I_s (A)	4.0×10^{-25}	2.1×10^{-25}	1.6×10^{-26}	7.0×10^{-28}	6.4×10^{-28}	3.2×10^{-28}
	n	1.20	1.18	1.12	1.07	1.07	1.06
$V_{j,th}$	(V)	1.460	1.470	1.470	1.472	1.476	1.480
D_{nr1}	I_s (A)	4.0×10^{-23}	6.0×10^{-22}	8.0×10^{-20}	9.0×10^{-20}	1.0×10^{-19}	1.4×10^{-19}
	n	1.30	1.40	1.60	1.60	1.60	1.60
R_{nr1}	(Ω)	300	300	200	50	50	50
D_{nr2}	I_s (A)	2.0×10^{-18}	5.0×10^{-17}	1.5×10^{-16}	3.0×10^{-15}	2.0×10^{-14}	9.0×10^{-11}
	n	2.00	2.10	2.150	2.30	2.50	3.70
R_{nr2}	(Ω)	1.0×10^{5}	6.0×10^{4}	4.0×10^{4}	1.5×10^{4}	1.5×10^{4}	1.8×10^{3}
D_{lk}	I_s (A)	6.0×10^{-17}	1.5×10^{-14}	1.0×10^{-12}	1.5×10^{-11}	5.0×10^{-10}	6.0×10^{-10}
	n	3.00	3.70	6.40	6.40	6.40	6.40
R_{lk}	(Ω)	1.0×10^{9}	1.0×10^{9}	5.0×10^{8}	1.0×10^{8}	1.2×10^{7}	1.5×10^{6}
R_p	(Ω)	1.0×10^{14}	8.0×10^{12}	3.0×10^{11}	3.0×10^{9}	2.0×10^{8}	3.0×10^{7}
R_s	R_c (Ω)	31	31	31	32	32	32
	R_{n0} (Ω)	50	55	55	55	55	55
	I_{n0} (mA)	6.5	6.5	6.5	6.5	6.5	7.5

decrease. The threshold junction voltage $V_{j,th}$ is 1.46 V in the initial state [18], and it increases with further increases in the ESD voltage. After the application of 1,000 V ESD pulses, $V_{j,th}$ increases to 1.47 and further increases to 1.48 V when the ESD voltage is 5,800 V. Since $V_{j,th}$ is logarithmically proportional to the injected carrier concentration [19], the ESD-induced degradation of oxide VCSELs increases the threshold carrier concentration required to reach the lasing threshold, indicating that optical absorption increases with the ESD accumulation.

The portion of the nonradiative recombination current I_{nr1} and I_{nr2} in the total current becomes greater as the applied ESD pulse amplitude increases. The reverse saturation current of the diode D_{nr1}, which represents the nonradiative current I_{nr1}, increases from 4.0×10^{-23} to 6.0×10^{-22} A and 1.4×10^{-19} A after the application of 1,000 V and 5,800 V ESD pulses. The ideality factor of D_{nr1} increases from 1.3 to 1.4 and 1.6 after the applications of 1,000 V and 5,800 V ESD pulses. The resistor R_{nr1} series connected to the diode D_{nr1} decreases from the initial value of 300 Ω to 50 Ω after the application of 2,400 V pulses and shows no further decrease with the further increase in the ESD voltage beyond 2,400 V. For the diode D_{nr2} which provides a current path for the nonradiative current I_{nr2}, the saturation current increases from 2.0×10^{-18} A in the initial state to 5.0×10^{-17} and 9.0×10^{-11} A after the application of 1,000 V and 5,800 V ESD pulses, showing 1.8×10^{6} times increase compared to the initial value. The ideality factor of D_{nr2} increases from 2 in the initial state to 2.1 and 3.7 after the application of 1,000 V and 5,800 V ESD pulses. This increase in nonradiative current components and optical loss shows that degradation takes place in the entire active area for the ESD voltage of 5,800 V. On the other hand, the resistor R_{nr2} decreases from the initial value of 100 kΩ to 60 kΩ after the application of 1,000 V ESD pulses and further decreases to 1.8 kΩ after the application of 5,800 V ESD pulses. The nonradiative current components I_{nr1} and I_{nr2} show a similar rate of increase at the beginning of the degradation; however, I_{nr2} leads the change in I-V characteristics after the application of 3,600 V ESD pulses.

Figures 7 (a) and (b) show the calculated current components and the fitted and measured I-V and I-I (dV/dI) curves after the application of 3,600V ESD pulses. The fitted and measured curves are in good agreement, which demonstrates the validity of the current component analysis.

In summary, the development of forward ESD-induced degradation can be divided into the following three phases. In phase 1 before ESD-induced degradation starts, there is no change in the reverse current, dL/dI, and the threshold current. In phase 2 after ESD-induced degradation starts but is confined to the edge of the active area, the reverse current increases, while the deterioration of the dL/dI and threshold current is

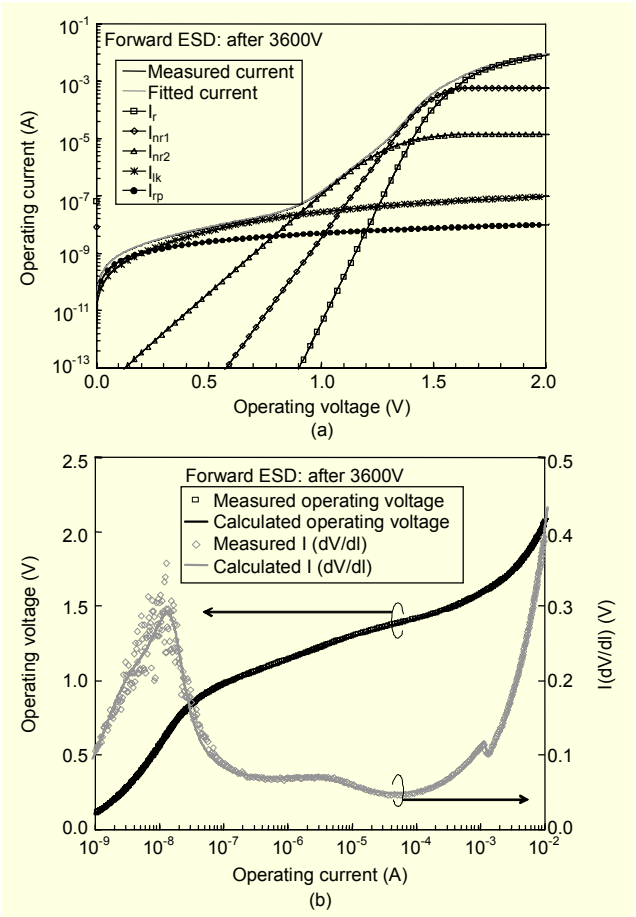

Fig. 7. Measured and numerically fitted I-V and I-I (*dV*/*dI*) curves of the tested device after the application of 3,600 V ESD pulses during forward ESD pulse accumulation test: in (a) the black line and gray line denote the measured and fitted total current while the square, diamond, triangle, and asterisk lines denote the radiative, nonradiative, shunted diode, and resistive leakage current components, respectively. The black empty squares denote the measured I-V curve, while the gray empty diamonds denote the measured I-I (*dV*/*dI*). In (b), the black lines denote the numerically fitted I-V curves, and the gray lines denote the numerically fitted I-I (*dV*/*dI*) curves.

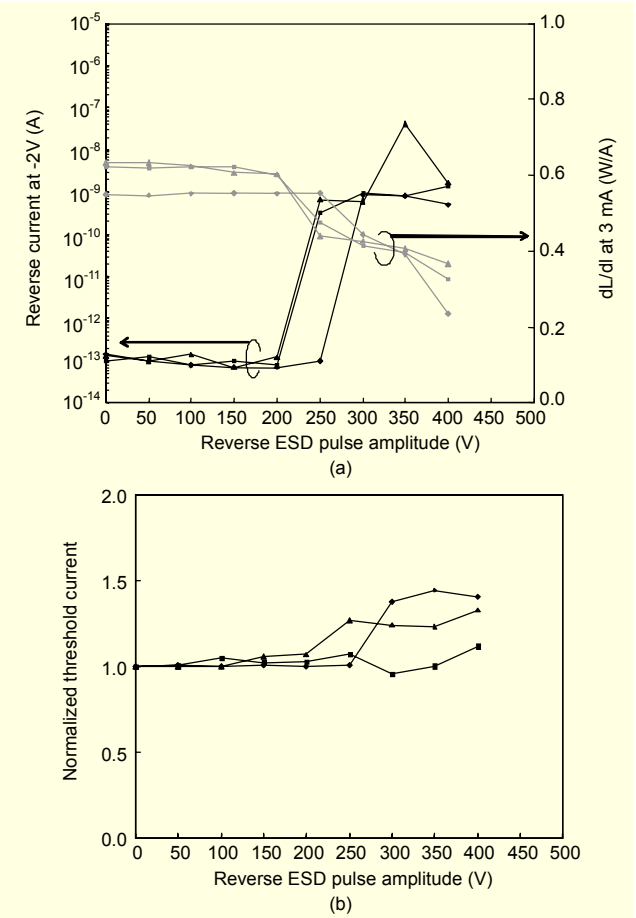

Fig. 8. Development of (a) the reverse current at the operating voltage of –2 V, and slope efficiency *dL*/*dI* at 3 mA and (b) the normalized threshold current of three different devices during the reverse ESD pulse accumulation test. The black lines denote the development of the reverse current, while the gray lines denote the development of *dL*/*dI* in (a).

relatively slow after the first sudden degradation. In phase 3 after serious ESD-induced degradation all over the active area, the reverse current keeps increasing, *dL/dI* decreases sharply, and the threshold current increases abruptly.

4. Development of Reverse ESD-Induced Degradation

The development of reverse ESD-induced degradation showed a different behavior than forward ESD-induced degradation. Figure 8(a) shows the reverse current at the operating voltage of –2 V and *dL/dI* at the operating current of 3 mA in terms of the reverse ESD voltage. Up to an ESD voltage of –200 V, the reverse current at the operating voltage of –2 V stayed around 0.1 pA and did not change compared to the initial value. After applying –250 V pulses, the reverse current at the operating voltage of –2 V drastically increased up to about 1 nA for two of the devices and increased for the other device at –300 V. Once the reverse current jumped to the 1 nA range, further increase of the ESD voltage up to –400 V did not increase the reverse current significantly. This is in good agreement with the EL images shown in Fig. 3(c) where there are no newly generated dark spots after the application of ESD threshold pulses. The slope efficiency *dL/dI* at the operating current of 3 mA simultaneously decreased with the increase in the reverse current. The decrement of *dL/dI* at the operating current of 3 mA after application of reverse ESD threshold pulses is greater than that of the forward ESD pulse accumulation test. After the first decrease of *dL/dI*, the slope efficiency gradually decreased as the reverse ESD voltage increased. The threshold current started to increase at –250 V

for two of the devices and increased at –300 V for the other device (see Fig. 8(b)). However, the threshold current may not show any notable increase in spite of further increase in the ESD voltage.

We could not observe any reverse ESD-induced degradation below the ESD threshold of about –250 V, and then, degradation abruptly occurred at the ESD threshold voltage, leading to a decrease in the slope efficiency simultaneously with increases in the reverse leakage and the threshold current in some cases. The reverse ESD-induced increment of the reverse current is approximately one hundred times greater and the reduction ratio of *dL/dI* at the ESD threshold is about two times higher than those of the forward ESD-induced degradation. In other words, the degradation induced by reverse ESD occurs suddenly at the ESD threshold voltage with no symptom, and the degree of degradation is more serious than the degradation induced by forward ESD. However, the reverse ESD-induced degradation tends to saturate in contrast to the degradation induced by forward ESD.

These results can be summarized as follows. The development of the electro-optical characteristics during the reverse ESD pulse accumulation is divided into two phases. In phase 1 below the ESD threshold and before reverse ESD-induced degradation starts, there is no change in the reverse current, *dL/dI*, the threshold current, and so on. In phase 2 above the ESD threshold and after degradation starts, the reverse current abruptly increases with the simultaneous decrease in *dL/dI*. The threshold current may not increase in some devices.

IV. Conclusion

We investigated the effects of forward and reverse ESD on oxide VCSELs, focusing on changes in and development of electro-optical characteristics. Both forward and reverse ESD-induced degradation caused the leakage current, threshold current, and series resistance to increase and simultaneously caused the slope efficiency to decrease and effective active area to be reduced. However, reverse ESD causes more sudden and abrupt degradation than forward ESD pulses. The degradation induced by forward ESD pulse accumulation is divided into three different phases, while the degradation caused by reverse ESD pulse accumulation is divided into two phases. The transitions between each degradation phase appear with the discernible decrease in the slope efficiency and the increase in the threshold and leakage current, although the threshold current may decrease in some devices. Also, the number of spatial modes decreases since the effective active area is reduced with the degradation. Both the initial forward and reverse ESD-induced degradation starts with the sudden decrease in the slope efficiency simultaneously with the increase in the reverse current. The increase in the threshold current is mainly due to increased nonradiative recombination current, while the decrease in the slope efficiency results from the increased optical absorption which is indicated by the increased threshold voltage $V_{j,th}$. Increased leakage current at operating voltages below 0.5 V results mainly from increased resistive leakage and can be used as an indicator of ESD-induced degradation.

References

[1] H. Mizuno et al., "Replicated Polymeric Optical Waveguide Devices with Large Core Connectable on Plastic Optical Fiber Using Thermo-plastic and Thermo-curable Resins," *J. Lightwave Technol.*, vol. 24, no. 2, Feb. 2006, pp. 919-926.

[2] Å. Haglund et al., "Comparative Study of the High-Speed Digital Modulation Performance of Single- and Multi-mode Oxide Confined VCSELs for Free Space Optical Interconnects," *Proc. SPIE*, vol. 4649, 2002, pp. 272-280.

[3] M. Gruber, R. Kerssenfischer, and J. Jahns, "Planar-Integrated Free-Space Optical Fan-Out Module for MT-Connected Fiber Ribbons," *J. Lightwave Technol.*, vol. 22, no. 9, Sept. 2004, pp. 2218-2222.

[4] A. Chow et al., "Smart Optical Sensors for Industrial and Consumer Applications," *Proc. ESTC*, Sept. 2006, pp. 101-106.

[5] L.F. DeChiaro and C.J. Sandroff, "Improvement in Electrostatic Discharge Performance of InGaAsP Semiconductor Lasers by Facet Passivation," *IEEE Trans. Electron Device*, vol. 39, no. 3, Mar. 1992, pp. 561-565

[6] J. Jeong, K.H. Park, and H.M. Park, "Wavelength Shifts of 1.5-mm DFB Lasers Due to Human-Body-Model Electronic Discharge Followed by Accelerated Aging Experiments," *J. Lightwave Technol.*, vol. 13, no. 2, Feb. 1995, pp. 186-190.

[7] H. Ichikawa et al., "Analysis on ESD-Induced Degradation of GaInAsP LD," *SEI Technical Review*, no. 64, Apr. 2007, pp. 9-14.

[8] J.-S. Huang, T. Olson, and E. Isip, "Human-Body-Model Electrostatic Discharge and Electrical-Overstress Studies of Buried-Heterostructure Semiconductor Lasers," *IEEE Trans. Device and Mater. Rel.*, vol. 7, no. 3, Sept. 2007, pp. 453-461.

[9] B. M. Hawkins et al., "Reliability of Various Size Oxide Aperture VCSELs," *Proc. ECTC*, May 2002, pp. 540-550.

[10] S.A. McHugo et al., "Characterization of Failure Mechanisms for Oxide VCSELs," *Proc. SPIE*, vol. 4994, 2003, pp. 55-66.

[11] "Sensitivity Testing, Human Body Model, Component Level," ESD Association, Rome, ESD STM5.1, 2001.

[12] D. Mathes et al., "AOC Moving Forward: The Impact of Materials Behavior," *Proc. SPIE*, vol. 4994, 2003, pp. 162-172.

[13] J. Krueger et al., "Studies of ESD-Related Failure Patterns of Agilent Oxide VCSELs," *Proc. SPIE*, vol. 4994, 2003, pp. 162-

172.
[14] C. Helms et al., "Reliability of Oxide VCSELs at Emcore," *Proc. SPIE*, vol. 5364, 2004, pp. 183-189.
[15] H.C. Neitzert, A. Piccirillo, and B. Gobbi, "Sensitivity of Proton Implanted VCSELs to Electrostatic Discharge Pulses," *IEEE J. Quantum Electron.,* vol. 7, no. 2, Mar. 2001, pp. 231-241.
[16] P.D. Wright, "Electrical Derivative Characteristics of InGaAsP Buried Heterostructure Lasers," *J. Appl. Phys.*, vol. 61, Mar. 1987, pp. 1720-1724.
[17] A. Ramaswamy et al., "Electrical Characteristics of Proton-Implanted Vertical-Cavity Surface-Emitting Lasers," *IEEE J. Quantum Electron.,* vol. 34, no. 11, Nov. 1998, pp. 2233-2240.
[18] P.A. Barnes and T.L. Paoli, "Derivative Measurements of the Current-Voltage Characteristics of Double-Heterostructure Injection Lasers," *J. Quantum Electron.,* vol. QE-12, Oct. 1976, pp. 633-639.
[19] W.B. Joyce and R.W. Dixon, "Electrical Characterization of Heterostructure Laser," *J. Appl. Phys.*, vol. 49, July 1978, pp. 3719-3728.

Taeyong Kim received the BS and MS degrees in electrical and computer engineering from Ajou University, Suwon, Korea, in 2001 and 2003, respectively, where he is currently working toward the PhD degree. His research focuses on the structure design and analysis of the electrical and optical characteristics of vertical-cavity semiconductor laser diodes.

Taeki Kim received the BS degree in electrical and computer engineering from Ajou University, Suwon, Korea, in 2006, and he will receive the MS degree in electrical and computer engineering from Ajou University, Suwon, Korea in 2008. He is studying the electrical and optical properties of vertical-cavity semiconductor diodes, including modulation characteristics.

Sangin Kim received the BS degree in electrical engineering from the Korea Advanced Institute of Science and Technology (KAIST), Daejeon, Korea in 1992. He received the MS and PhD degrees in electrical engineering from the University of Minnesota, Minneapolis-St. Paul, Minnesota, US, in 1995 and 1997, respectively. From 1997 to 2002, he was with Korea Telecom, where he had been involved in works on high capacity optical switching systems, optical access networks, and polarization mode dispersion compensation for high bit rate optical transmission. Currently, he is working as an associate professor in the Division of Electrical and Computer Engineering, Ajou University. His research interest covers broad spectrum of nanophotonics, guided wave optics, plasmonics, and photonic integrated circuits.

Sang-Bae Kim (S'81－M'87) received the BS degree in electrical engineering from Ajou University, Suwon, Korea, and MS and PhD degrees in electrical engineering from KAIST, Korea, in 1981, 1983, and 1987, respectively. From 1987 to 1990, he was with ETRI (Electronics and Telecommunication Research Institute), where he was involved in optoelectronic integrated circuits and diode lasers for optical communication. In 1990, he joined the faculty of Ajou University as an assistant professor, and is now a professor in the Division of Electrical and Computer Engineering. At present, he is involved in semiconductor optoelectronic devices including VCSELs, infrared and visible lasers, ultraviolet detectors, and LEDs. Also, he is actively involved in reforming engineering education; developing students' learning capabilities, assessing learning outcomes, and assessing program-level achievement.